ELSEVIER

Polymer 43 (2002) 2039–2048

polymer

www.elsevier.com/locate/polymer

Free volume-based modelling of free radical crosslinking polymerisation of unsaturated polyesters

Per B. Zetterlund*, Anthony F. Johnson

School of Chemistry, Interdisciplinary Research Centre in Polymer Science and Technology, University of Leeds, Leeds, LS2 9JT, West Yorkshire, UK

Received 27 September 2001; received in revised form 26 November 2001; accepted 3 December 2001

Abstract

A new mechanistic kinetic model is presented for the cure behaviour of unsaturated polyester (UP) resins. The model is based on free radical polymerisation mechanism and the free volume concept. The quasi steady-state assumption for the free radical concentration is not used, and the decrease in initiator efficiency with conversion and radical trapping are modelled separately. The glass transition temperature of partially cured samples was measured employing differential scanning calorimetry (DSC) in conjunction with dynamic mechanical analysis (DMA), and the values obtained were incorporated into the model. DSC obtained conversion-time data for a standard commercially available UP resin under isothermal conditions. The kinetic parameters of the model were estimated using parameter optimisation procedures resulting in good agreement between model predictions and experimental data. Modelling in combination with experimental cure data showed that at higher isothermal cure temperatures a greater extent of physical trapping of radicals occurs rendering them inactive.

Keywords: Free radical crosslinking; Free volume; Diffusion control

1. Introduction

Unsaturated polyester (UP) resins are of great commercial importance as low cost, high volume thermosetting matrix materials for composites produced by reaction injection moulding, injection moulding, compression moulding and pultrusion [1]. Linear UP's containing approximately 10 unsaturations per chain are usually transformed into a crosslinked network by free radical copolymerisation with a vinyl monomer such as styrene (St) in the presence of reinforcement, fillers and additives. Other commercially important crosslinkers include vinyl esters, dimethacrylates and divinyl benzene. The chemical cure process in these systems results in physical change as the resin is transformed from a fluid into a gel as gelation occurs, and vitrification may take place at high conversion as the glass transition temperature (T_g) increases. The cure of UP resins is accompanied by the formation of structural inhomogeneities (microgels) resulting from intramolecular crosslinking giving rise to spherical structures [2]. This process is one of the reasons that gelation occurs at higher levels of conversion than predicted by the Flory–Stockmeyer theory [3–5]. The kinetics of the process is affected by these physical changes as a result of diffusion controlled termination and propagation.

The development of a mechanistic model is a worthwhile exercise not only to obtain a predictive tool that is useful in process optimisation, but also to increase the fundamental understanding of these processes. Most available models are empirical [6–18] and are therefore of limited use as they can only be employed in a predictive manner within the experimental conditions for which the model parameters have been estimated. The non-empirical models based on radical mechanisms can be divided into two groups depending on how diffusion control is treated; (i) use of propagation rate coefficients that decrease empirically with increasing conversion [14,17,19–24], and (ii) use of the free volume concept [25,26]. Huang and Lee [25] proposed a cure model that involves the free volume concept to account for diffusion control. This model was later refined by Ma et al. [25] who calculated the change in free volume during cure as a function of the temperature and T_g. Both models invoked the quasi steady-state assumption for the free radical concentration, and made use of various lumped parameters in the optimisation procedures.

The work presented here [27] extends previously reported

* Corresponding author. Address: Department of Applied Chemistry, Graduate School of Engineering, Osaka City University, 3-3-138 Sugimoto, Sumiyoshi-ku, Osaka 558-8585, Japan. Tel.: +81-6-6605-2189; fax: +81-6-6605-2189.

E-mail address: pbzetterlund@a-chem.eng.osaka-cu.ac.jp (P.B. Zetterlund).

0032-3861/02/$ - see front matter
PII: S0032-3861(01)00789-3

free volume-based models [25,26] in a number of ways, essentially reducing the degree of empiricism and thereby increasing the predictive power. The quasi steady-state assumption for the free radical concentration is not invoked, and all unknown parameters are individually estimated, thereby making it possible to use the model to investigate the effect of individual parameter values on the predictions. The quality of the model predictions are judged not only in terms of conversion-time, but also by examining the fraction of trapped free radicals as a function of conversion. The decrease in initiator efficiency (f) with increasing degree of cure is treated separately from diffusion-controlled propagation.

2. Experimental

2.1. Materials

A commercially available UP resin (Resinous Chemicals Ltd, Ref. No. 1696/18) comprising maleic anhydride, phthalic anhydride (molar ratio maleic/phthalic = 2) and 1,2-propylene glycol together with St (35 wt%) was used. Benzoyl peroxide (BPO) (Aldrich Chemical Co. Ltd) was purified by extraction with acetone, reprecipitation in distilled water and drying under vacuum at room temperature prior to use (1 wt%).

2.2. Differential scanning calorimetry

Isothermal measurements of the rate of cure were carried out in an atmosphere of dry nitrogen by Differential scanning calorimetry (DSC) (Perkin Elmer Model DSC 7). Assuming that the specific heat capacity of the resin remains constant, the degree of cure α at time t can be obtained using Eq. (1):

$$\alpha(t) = \frac{1}{\Delta H_{\text{tot}}} \int_0^t \left(\frac{\mathrm{d}Q}{\mathrm{d}t} \right) \mathrm{d}t \tag{1}$$

where $(\mathrm{d}Q/\mathrm{d}t)$ is the DSC output in J g^{-1} min^{-1} and ΔH_{tot} is the total heat of cure in J g^{-1}. The value of ΔH_{tot} was calculated as -374 J g^{-1} based on the theoretical heat of copolymerisation of St with fumarate unsaturations in the prepolymer [28] of 69,000 J mol^{-1}. The DSC data were corrected for the heat of decomposition of the initiator by use of Eq. (2)

$$Q_{\text{c}} = Q - \Delta H_{\text{d}} \left(\frac{\mathrm{d}[I]}{\mathrm{d}t} \right) \tag{2}$$

where Q is the heat evolved in J g^{-1} min^{-1}, Q_{c} is the heat evolved corrected for the initiator decomposition and ΔH_{d} is the heat of decomposition of the initiator. The heat of decomposition of BPO has been reported [29] as -293 kJ mol^{-1}.

2.3. Dynamic mechanical analysis

Resin samples containing 1 wt% BPO were pre-cured to various degrees of conversion in the DSC at 80 °C. The reaction was stopped by quenching to 0 °C, and the partially cured resin was subjected to analysis by Dynamic mechanical analysis (DMA) (Perkin Elmer Model DMA 7) over the temperature range -60–200 °C under dry helium with a heating rate of 10 °C min^{-1} and a frequency of 1 Hz.

2.4. Computer simulations

A commercially available software package (VisSim Professional, Version 1.5d, Visual Solutions Inc.) was employed. Numerical integration was carried out using either the Euler or Backward Euler integration algorithms [30], and parameter optimisation by the Powell routine [31].

3. Cure model description

3.1. Assumptions

The assumptions made when deriving the present model were that; (i) all polymerisable double bonds are identical, and (ii) all free radicals are identical; (iii) all rate constants exhibit Arrhenius temperature dependence; (iv) there are no temperature or concentration gradients; (v) polymerisation shrinkage is proportional to the extent of cure; (vi) the rate of bimolecular termination is negligible. Reduced reaction rate curves were examined for different concentrations of crosslinking agent in an St/vinyl ester resin by Batch and Macosko [22]. Assumptions (i) and (ii) are reasonable if the polymerisation is close to the azeotropic composition [25]. It has been shown that for UP resins with similar composition to the resin used in the present study, this condition is satisfied reasonably well over most of the conversion range [32,33]. The disappearance of a plateau value with increasing crosslinking agent concentration is indicative of the rate of termination being negligible at these concentrations [22]. The UP resin of this study had a crosslinking agent concentration comparable to the highest concentration used by Batch and Macosko [22] and the reduced reaction rate (R_{r}) exhibited similar characteristics. The high crosslinking density in microgels creates significant steric hindrance for bimolecular termination [2]. Direct measurements by electron spin resonance spectroscopy (ESR) of free radical concentrations during UP resin cure support this notion; radical concentrations as high as 10^{-4} M have been detected [34]. This is significantly higher than the steady-state free radical concentration during conventional linear free radical polymerisation where concentrations are usually in the range 10^{-8}–10^{-6} M depending on the particular system and the reaction conditions [35], and reveals that the termination rate coefficient is significantly lower during the cure of UP resins. At the limiting conversion during isothermal UP resin cure in the temperature range 30–50 °C it has been

shown that the free radical concentration only decays by approximately 10% or less after storage for one month at room temperature [36], the radicals being physically trapped in the network structure and unable to terminate.

The concentrations of all participating species can be described by the rate equations for free radical polymerisation in the usual way:

$$d[I]/dt = -k_d[I] \quad (3)$$

$$d[R]/dt = 2fk_d[I] - k_z[Z][R] \quad (4)$$

$$d[Z]/dt = -k_z[Z][R] \quad (5)$$

$$d[M]/dt = -k_p[M][R] \quad (6)$$

3.2. Effective inhibitor concentration

Commercial UP resins contain a small, often unknown, amount of inhibitor to prevent premature reaction. Oxygen, another unknown quantity in most cases, can also act as an inhibitor. If the quasi steady-state assumption is made for the inhibition period and if the initial inhibitor concentration is small compared to the initial initiator concentration, the relationship shown in Eq. (7) between the effective inhibitor concentration $[Z]_{eff}$ and the inhibition time t_z can be derived [22]:

$$[Z]_{eff} = 2f[I]_0 k_d t_z \quad (7)$$

In this work, the value of $[Z]_{eff}$ was calculated using experimental values of t_z from isothermal DSC data.

3.3. Polymerisation shrinkage

The change in volume is the sum of the contributions from the polymerisation shrinkage and the thermal expansion/contraction, and has been reported to be approximately 13% as the cure reaction goes to completion ($\varepsilon = -0.13$, where ε is the fractional shrinkage at full conversion) for a commercial UP resin similar to the one employed in the present study [37]. The concentrations of all species except the inhibitor (the propagation rate is negligible before the inhibitor has been consumed) were corrected according to Eq. (8):

$$S_c = \frac{S}{1 + \varepsilon\alpha} \quad (8)$$

where S_c is the concentration corrected for the volume change ($S = [M]$, $[R]$, $[I]$), and α is monomer conversion.

3.4. Diffusion controlled kinetics

The equation derived by Huang and Lee [25] (Eq. (9)) was employed to describe the relationship between the propagation rate coefficient (k_p) and the monomer self-diffusion coefficient (D_M). It is assumed that each free radical chain end sweeps a sphere of constant volume and that the global rate of polymerisation is equal to the rate of polymerisation inside this sphere.

$$\frac{1}{k_p} = \frac{1}{k_{p0}} + \frac{C_1[R]}{D_M} \quad (9)$$

Here $C_1 = (v_s\delta_e)/A_e$, A_e is the mass transfer area, δ_e is the diffusion distance, v_s is the volume of the diffusion sphere, and k_{p0} is the propagation rate coefficient under chemical reaction control conditions.

3.5. Initiator efficiency (f)

The quantity f is defined as the fraction of radicals generated by initiator decomposition that initiate polymerisation, and is known to decrease with increasing conversion both in bulk and solution free radical polymerisation [38–42]. In this work, an empirical expression was employed [22]:

$$f = f_1 - (f_1 - f_2)\left(\frac{\alpha - \alpha_D}{\alpha_x - \alpha_D}\right) \quad (10)$$

where f_1 is the value of f at zero conversion ($f_1 = 0.6$), f_2 is the final value ($f_2 = 0$), α_D is the conversion at the onset of the diffusion-limited zone (the conversion level at which propagation becomes diffusion controlled and/or f begins to decrease), and α_x is the conversion at which $f = f_2$. This empirical model predicts that f increases with increasing temperature, a finding which is in accord with published experimental results [40]. The procedures used to evaluate the parameters of Eq. (10) and the temperature dependence of α_x are described in Appendix A.

3.6. Free volume

In previous reports [16,17], the free volume theory of Bueche [44] has been employed to describe experimental observations. Here, the free volume theories of Cohen–Turnbull [43] (Eq. (11)) and Bueche (Eq. (12)) have been used in separate simulations to express the diffusion coefficients in terms of the free volume of the system.

$$D = \frac{C_1}{A_1}\exp\left(-\frac{\gamma V^*}{V_f}\right) \quad (11)$$

In Eq. (11) A_1 is a parameter which is function of the molecular diameter as well as the gas kinetic velocity and a geometric factor, γ is a correction factor ($0.5 < \gamma < 1$), V_f is the free volume, and V^* is the critical free volume (the minimum volume required for displacement of a sphere).

$$D = \frac{C_1}{A_2}\exp\left(-\frac{V^*}{V_f}\left[\ln\left(\frac{V^*}{V_f}\right) - 1\right]\right) \quad (12)$$

In Eq. (12), A_2 is also a constant appropriate for any given liquid. The essential difference between the Cohen–Turnbull [43] and Bueche [44] models is that the latter assumes that the free volume packets are of the same size whereas the former does not.

In Eqs. (11) and (12), V_f is the total fractional free volume

of the system. A critical fractional free volume (V^*) for a molecular system can be defined as shown in Eq. (13)

$$V^* = \frac{nv^*}{V_{tot}} \tag{13}$$

in which n is the number of polymer segments, V_{tot} is the total volume of the system, and v^* is the critical free volume needed for a chain segment jump (i.e. diffusion) to occur.

The value of V_f was computed from the glass transition temperature (T_g) of the partially cured resin [26] by use of the Simha–Boyer equations [45,46].

$$V_f = V_{fg} + \beta_l(T - T_g) \qquad \text{for } T > T_g \tag{14}$$

$$V_f = V_{fg} + \beta_g(T - T_g) \qquad \text{for } T < T_g \tag{15}$$

$$\beta_l = \frac{0.164}{T_g} \tag{16}$$

$$\beta_g = \beta_l - \frac{0.113}{T_g} \tag{17}$$

In these equations, β_l and β_g are the thermal expansion coefficients for the liquid and glassy states, respectively.

3.7. Glass transition temperature

The following equation describing the relationship between the degree of cure and T_g was originally proposed for stepwise polymerisation and has been successfully employed to the cure of UP resins [22,47,48]:

$$\frac{1}{T_g} = \frac{1}{T_{g0}} - a\alpha \tag{18}$$

where T_{g0} is T_g at $\alpha = 0$ and the parameter a is a constant. The existence of a master curve for T_g as a function of conversion for UP resin systems has been verified experimentally, and this includes a resin with the same composition as that employed in the present study [49,50]. Without this being the case, Eq. (18) cannot be used in the cure model at different temperatures.

During dynamic DMA measurements on partially polymerised samples, the cure reaction starts in the DMA pan when devitrification occurs as $T > T_g$. As the conversion increases, $T_g > T$ and vitrification will occur. As T is increased further, devitrification takes place and reaction proceeds until a limiting conversion is reached. This pattern of behaviour give rise to a rather complex storage and loss moduli pattern as a function of T. This process (heating rate = 10 K min^{-1}) was simulated using the cure model of Han and Lee [20] (with $[M]_\infty = 0.75$ and $f = 0.6$), computing T_g from Eq. (18) (using the values of a and T_{g0} as obtained later in this study—Fig. 1). The lines corresponding to T_g of the samples cross the experimental temperature plot three times over the temperature range scanned. The first T_g detected corresponds to that of the pre-cured sample.

The experimentally obtained loss tangent and loss moduli exhibit two peaks in agreement with the simulations [50] (Fig. 2). The first loss modulus and loss tangent peaks became broader as the level of pre-cure was increased. This has been ascribed to increasing inhomogeneity with conversion [49]. The T_g observed is some average value corresponding to different zones, each with its own relaxation characteristics. The position of the second peak remained approximately constant and independent of the degree of pre-cure, in agreement with the simulations (Fig. 1) which indicated that devitrification occurs after the final T_g has been reached i.e. corresponding to the final degree of conversion. The T_g's of the pre-cured samples were defined as T at the peak of the first maximum of the loss modulus. Eq. (18) was successfully fitted to the results, giving $a = 1.862 \times 10^{-3}$ (Fig. 3).

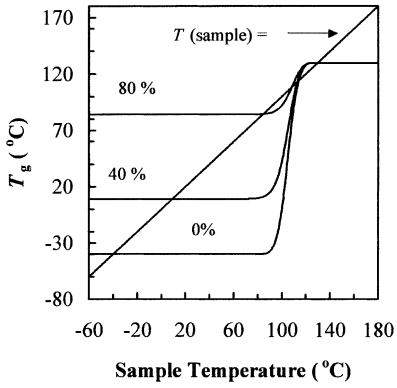

Fig. 1. Simulated T_g vs. sample temperature during UP resin cure at a heating rate of 10 K min^{-1} using the cure model of Han and Lee [20], with T_g from Eq. (18) (using the values of a and T_{g0} as obtained in this study).

3.8. Parameter optimisation

The unknown parameters (k_{p0} and (A_2 and V^*) or (A_1 and γV^*)) were estimated using standard curve fitting procedures to match experimental DSC data. The input parameter values used are shown in Table 1. It has been shown that higher accuracy is obtained by fitting the conversion

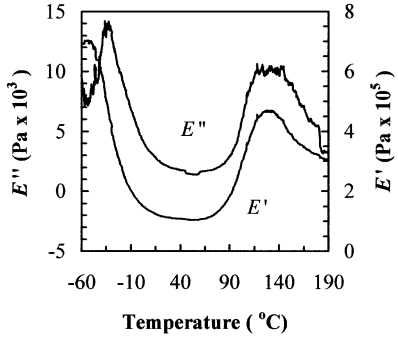

Fig. 2. E' and E'' as functions of curing temperature during cure at a heating rate of 10 K min^{-1} for a sample with an initial degree of cure of 0.10.

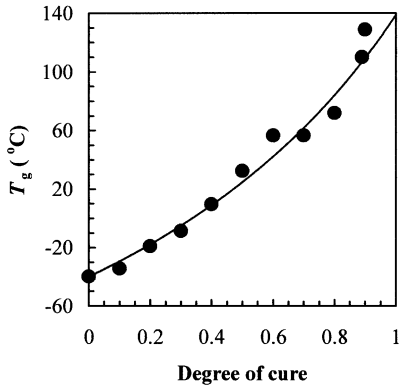

Fig. 3. Experimentally obtained T_g as a function of the degree of cure.

rather than the rate of conversion [52], hence, this approach was adopted in this work. In order to minimise the well-known problem of multiple solutions in the parameter optimisation procedures, additional independent criteria are desirable. The criterion selected was the active free radical fraction (F), one previously introduced by Batch and Macosko [22]. Batch and Macosko [22] considered diffusion resistance to be the result of free radicals becoming trapped in the 3D network and thus becoming unable to react in situations where molecular mobility is low. The fraction of active (i.e. not trapped) radicals was modelled by multiplying the free radical concentration (Eqs. (4)–(6)) with the empirical function F which decreases from 1 to 0 with increasing conversion. The shape of F was found from Eq. (19) by replacing $[R]$ with $F[R]$ and solving for F:

$$F = \left(\frac{d\alpha}{dt}\right)\frac{1}{(1-\alpha)k_{p0}[R]} \tag{19}$$

This procedure only yields the relative change in F with conversion since k_{p0} is unknown. The quantities $d\alpha/dt$ and α can be obtained experimentally, and $[R]$ can be computed from Eqs. (3)–(5). The value of F can also be computed directly from the model (i.e. by using $d\alpha/dt$ and α from the model and not from DSC data) by rearrangement of Eq. (20), recognising that $F = k_{p0}/k_p$ (Eq. (21)):

$$\frac{d\alpha}{dt} = k_p[R](1-\alpha) = k_{p0}F[R](1-\alpha) \tag{20}$$

Table 1
Parameters for optimisations

Parameter	
$[M]_0$	6.063 mol dm^{-3}
$[I]_0$	0.0471 mol dm^{-3}
$[Z]_0 = [Z]_{eff}$	1.43×10^{-4} mol dm^{-3}
E_d [28]	119,600 J mol^{-1}
A_d [28]	9.32×10^{14} min^{-1}
E_z [51]	70,464 J mol^{-1}
A_z [51]	1.06×10^{14} dm^3 mol^{-1} min^{-1}

$$F = \frac{k_p}{k_{p0}} = \frac{1}{\left(1 + \dfrac{k_{p0}C_1[R]}{D_M}\right)}k_p[R](1-\alpha) \tag{21}$$

The range $0 < \alpha < 0.10$ was excluded from this part of the overall fitting procedure as the experimental data are less accurate in this region (due to the initial temperature ramp, hence, F was set equal to one when $\alpha = 0.10$), and the model prediction of $[R]$ is very sensitive to the model parameters at low conversion. The values of F as a function of conversion calculated using Eqs. (19) and (21) could thus be used as an additional means of estimation of the model parameters.

In summary, the model parameters were evaluated using the following procedures: (i) model fitting to the experimental conversion (isothermal data) using a range of fixed values of γV^* and V^* (employing the Cohen–Turnbull [43] and Bueche [44] free volume theories separately) with respect to k_{p0} and A_1 or A_2, thus finding a range of values of γV^* and V^* that gave conversion predictions of comparably high quality; (ii) for each temperature, the values of γV^* and V^* that resulted in the smallest residual area between the values of F from Eqs. (19) and (21) were selected. In each case, the best agreement with regards to the F curves coincided with the best conversion prediction in terms of γV^* and V^*, although the difference in quality between many conversion predictions was very small; (iii) curve fitting with respect to k_{p0} and A_1 or A_2 with γV^* and V^* fixed at their optimum values in terms of the F curves.

4. Results and discussion

Preliminary optimisations indicated that the Cohen–Turnbull [43] approach resulted in better model predictions, and the optimisations using this approach were, therefore, somewhat more extensive than for the Bueche [44] approach.

4.1. Cohen–turnbull free volume theory

Conversion predictions of very similar quality could be obtained with a range of values of γV^* (Fig. 4). However, the corresponding simulated values of F reveal a strong dependence on γV^*, thus providing the necessary criterion for the selection of a value of γV^* for each temperature (Fig. 5). The most satisfactory F fits were obtained with $0.15 < \gamma V^* < 0.40$ for all temperatures investigated. The full results of the optimisations are displayed in Table 2. The values of γV^* giving the best fit to F data go through a minimum for each temperature as the temperature is increased. The Arrhenius plot of k_{p0} deviated from linearity in the temperature range 105–120 °C when the best values of γV^* were used in the optimisation procedures for reasons which are thought to relate to the existence of multiple solutions in the optimisation procedures. If the parameter A_1 is overestimated at high temperature, this will result in

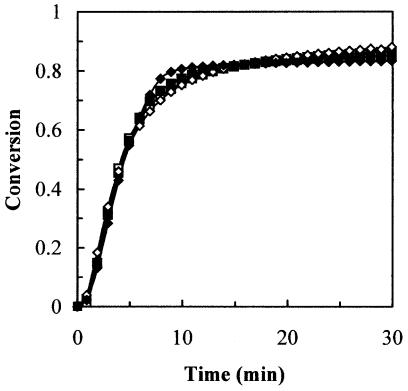

Fig. 4. Model predictions of conversion from optimisations using fixed values of γV^* at 95 °C (Cohen–Turnbull approach). □ DSC, $\gamma V^* = 0.10$ (◇), 0.21 (■) and 0.70 (◆).

underestimation of k_{p0}. The linear portion of the plot yielded the following: $E_p = 59,720$ J mol^{-1} and $A_p = 6.32 \times 10^{10}$ M^{-1} min^{-1} (Fig. 6). These fall within the wide range of values previously reported [19–21,53]. The model predictions obtained with the optimised values of γV^*, A_1 and k_{p0} obtained using the Arrhenius parameters are displayed with the experimental conversion in Fig. 7. It can be seen that the level of agreement is satisfactory.

4.2. The free volume theory of Bueche

The parameter optimisations revealed that the best fits were achieved when $0.15 < V^* < 0.30$ (Table 2). The optimum values of V^* did not go through a minimum with increasing temperature as in the case of Cohen–Turnbull [43] approach, but kept increasing. The Arrhenius plot of k_{p0} (using the best value of V^* for each temperature) was similar to that with the Cohen–Turnbull [43] approach (Fig. 6). As before, the data point at 120 °C was considered anomalous and was excluded for the reasons explained earlier. The resulting values obtained were: $E_p = 64,210$ J mol^{-1} and $A_p = 2.65 \times 10^{11}$ M^{-1} min^{-1}. The value of A_2 decreased with increasing temperature and

Table 2
Results of optimisation procedures and the parameter α_D

Temperature (°C)	A_1	γV^*	A_2	V^*	α_D
120	1.94×10^{-3}	0.33	2.73×10^{-2}	0.26	0.014
115	2.88×10^{-3}	0.30			0.0028
110	6.50×10^{-3}	0.27			0.013
105	1.24×10^{-2}	0.25			0.029
100	1.72×10^{-2}	0.21	2.87×10^{-1}	0.17	0.013
95	2.24×10^{-2}	0.21			0.017
90	2.05×10^{-2}	0.19			0.014
85	1.16×10^{-1}	0.16	3.16×10^{-1}	0.16	0.016
80	2.46×10^{-2}	0.21			0.025
75	2.53×10^{-3}	0.31	2.05	0.16	0.014

was approximately one order of magnitude greater than the value of A_1 obtained from the Cohen–Turnbull [43] approach as a result of the term $\ln(V^*/V_f) - 1$ which appears in Eq. (12) of the Bueche approach. The model predictions, using optimised values for V^*, A_2 and k_{p0} (calculated from the Arrhenius parameters), reveal satisfactory agreement with experimental data, but not as good as that achieved with the Cohen–Turnbull model at higher temperatures (Fig. 8).

The pre-exponential factor of the expression for the diffusion coefficient is a function of the jump distance (the average change in distance between two equilibrium positions of a diffusing segment), the jump frequency (the number of times a diffusing species changes its equilibrium position per unit time), the molecular weight, and the extent of entanglements present [44]. Hence, it would be expected that A_1 and A_2 are functions of both temperature and degree of cure. They would also be expected to decrease with increasing temperature with a resultant increase in the diffusion coefficient. Huang and Lee [25] and Ma et al. [26] both assumed that A_2 is a function of temperature only and that it decreases with increasing temperature with an Arrhenius temperature dependence. The estimated values of A_2 and A_1 are in qualitative agreement with the earlier reasoning, with the exception of the low values of A_1

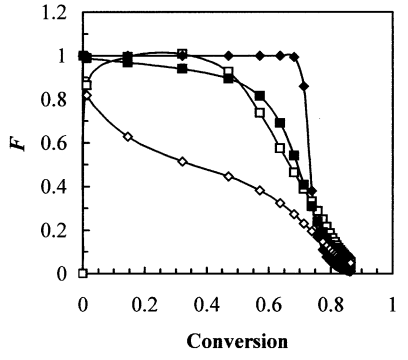

Fig. 5. Model predictions of F vs. conversion using fixed values of V^* at 95 °C (Cohen–Turnbull approach). □ DSC, $\gamma V^* = 0.10$ (◇), 0.21 (■) and 0.70 (◆).

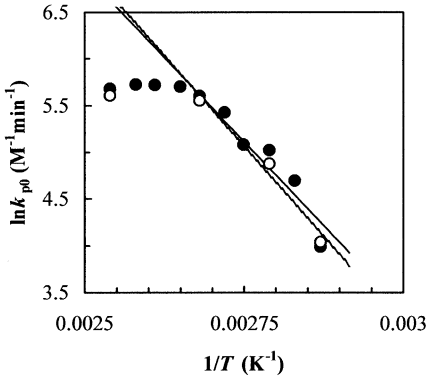

Fig. 6. Arrhenius plot of k_{p0} obtained from parameter optimisation procedures. ○ Bueche, ● Cohen–Turnbull.

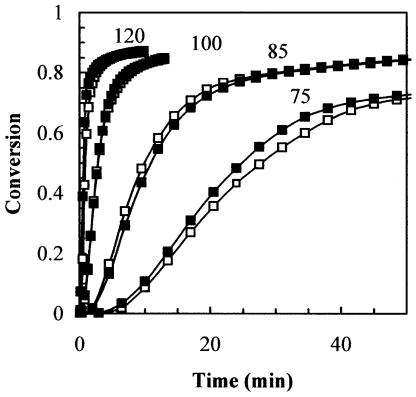

Fig. 7. Model predictions of conversion (Cohen–Turnbull) with k_{p0} from the Arrhenius plot compared with DSC data. □ DSC, ■ Model.

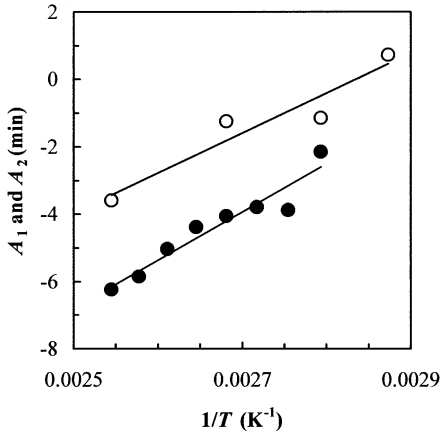

Fig. 9. Arrhenius plots of A_1 and A_2. ○ Bueche, ● Cohen–Turnbull.

at the two lowest temperatures. However, since the unsaturations are distributed between many different molecular weight species, including St, and that this changes with time, the estimated values of A_1 and A_2 must be considered to be some form of average value for the entire conversion range. The pre-exponential factor of the diffusion expression is thus only an approximation for the whole cure range, and, furthermore, the behaviour of C_1 is not known. These facts, together with the approximation that γV^* and V^* are constant with conversion, makes more detailed speculation fruitless. Arrhenius plots for the linear data of A_1 and A_2 yields activation energies of 118,000 J mol^{-1} (Cohen–Turnbull [43]) and 98,135 J mol^{-1} (Bueche [44]), i.e. somewhat higher than that obtained by Huang and Lee [25] (48,406 J mol^{-1}) but close to the value reported by Ma et al. [26] (92,848 J mol^{-1}); both groups of authors used the Bueche theory (Fig. 9).

Huang and Lee [25] and Ma et al. [26] estimated V^* to be 0.09, close to the values obtained in this study. According to Bueche [44], $\ln(V^*/V_f) - 1 \approx 1$. For the UP resin employed in this study, the average V_f throughout the cure process is close to 0.07 as predicted by the cure model using the Cohen–Turnbull approach, leading to $V^* \approx 0.52$. Cohen and Turnbull [43] stated that $V^* \approx 10V_f$, and a similar result has been obtained here. However, since the nature of the diffusing species change as the cure reaction proceeds, it might be expected that the critical free volume also changes with conversion.

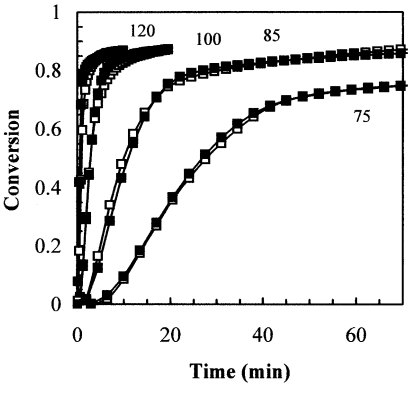

Fig. 8. Model predictions of conversion (Bueche) with k_{p0} from the Arrhenius plot compared with DSC data. □ DSC, ■ Model.

4.3. Final degree of cure

The termination reaction in linear free radical bulk polymerisation of St is controlled by translational diffusion from, arguably, approximately 20% conversion onwards, and this remains the rate determining step until reaction diffusion becomes the predominant mode of termination at higher conversion levels [54–57]. The viscosity in a curing UP resin system will be considerably higher than in the bulk polymerisation of St, and it would thus appear likely that any polymer–polymer reaction will be controlled by translational diffusion. The reaction of fumarate groups requires translational diffusion by polymer segments, i.e. it is a polymer–polymer reaction as opposed to the propagation of St monomer where the diffusing species are small St molecules. From these considerations one would anticipate that the fraction of reacted unsaturation relative to the fraction of reacted St would increase with increasing temperature.

Horie et al. [58] measured the storage modulus and found that it increased with increasing isothermal cure temperature. A maximum in the final conversion as a function of isothermal cure temperature was observed, and the activation energy for reaction of UP segments was estimated to be higher than that of St monomer. Further experimental evidence has been reported by Dell'Erba et al. [33]. It is interesting to note from their reported data that the final conversion of fumarate to that of St increased from 0.83 to 0.93 as the temperature was increased from 63 to 90 °C. The net result is that described by Horie [58]. At the same conversion reached at two different temperatures, the sample cured at the higher temperature has a higher density of crosslinks. At some temperature, the rate of

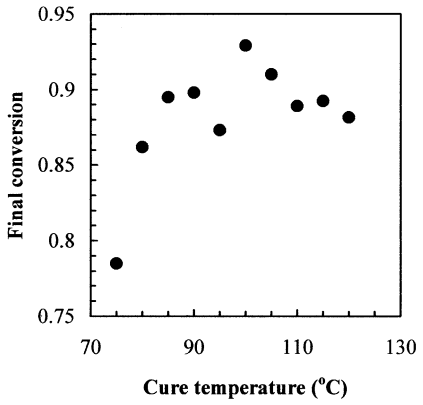

Fig. 10. Final degree of cure from DSC measurements vs. isothermal curing temperature.

propagation will become negligible i.e. the temperature at which the density of crosslinks prevents monomer diffusion. Concurrently, the increasing temperature leads to higher monomer diffusion rates, which increases the final level of cure. It is the combination of these two mechanisms, which lead to the maximum in the final level of cure.

The final degrees of cure obtained in the present study display a maximum in agreement with the earlier reasoning (Fig. 10). The dependence of the crosslink density on temperature and conversion should also be reflected in the value of F. The results from Eq. (19) (using the f-expression of Eq. (10) and $d\alpha/dt$ and α from DSC data) clearly show that F decreases as expected as the temperature is increased over the conversion range (Fig. 11). Radical trapping on a large scale is believed to commence after the maximum in R_r, and this point (α_R) was estimated from the experimental data to lie between 0.31 and 0.41 (see Appendix A). The trends in F support this notion, indicating that significant trapping commences after a conversion of approximately 0.40.

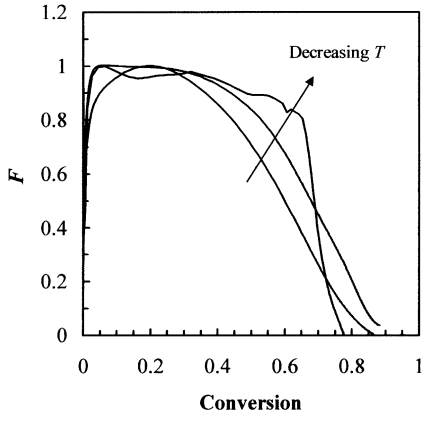

Fig. 11. F vs. conversion from Eqs. (10) and (19) and DSC data for the curing temperatures 75, 105, and 120 °C.

5. Conclusions

A new mechanistic kinetic model has been developed for the free radical crosslinking reaction of UP resins which extends previous understanding of cure processes that invokes free volume concepts to explain high conversion behaviour. Good agreement has been obtained between model predictions and experimental kinetic data obtained by DSC using both the Bueche [44] and Cohen–Turnbull [43] approaches to free volume, with somewhat better results being obtained using the latter. A semi-empirical approach to the decrease in initiator efficiency (f) with increasing conversion made it possible to demonstrate that the value of f increases with increasing cure temperature. Modelling studies, in combination with experimental cure data, have shown that isothermal cure at higher temperatures results in greater extents of physical trapping of radicals at a given degree of cure, which is consistent with other recent studies of bulk free radical polymerisation studies with St where crosslinking takes place. The model is generic and can be used for predictive purposes for the cure behaviour of UP systems other than the one which has been the focus of these studies, provided the necessary physical and kinetic parameters are available.

Appendix A. Initiator efficiency

An empirical expression for f as a function of temperature and conversion was developed by comparing the conversion-dependence of the model prediction of F (which is a function of f) with the experimental R_r curve, bearing in mind that radical trapping on a large scale is thought to begin after the maximum, α_R, in the R_r curve. The value of F was computed from Eqs. (3)–(5) and (19) for different expressions of f, using the initial concentrations and rate constants in Table 1, and α and $d\alpha/dt$ from DSC data. The value of f at very high conversion has previously been shown to be extremely low [38,39]. The value of α_R was estimated experimentally to lie between 0.31 and 0.41 without any clear trend with temperature. The value of f was assumed to decrease linearly with conversion from $f_1 = 0.6$ at the onset of the diffusion-limited zone ($\alpha = \alpha_D$) [22], to $f_2 = 0$ at $\alpha = \alpha_X$ (Eq. (10)). The parameter α_D was defined as the conversion at which $d(R_r)/dt$ starts to decrease, and was estimated graphically (Table 2). Normalised R_r vs. normalised time curves ($R_r/R_{r,max}$ vs. t/t_{final}) computed from Eq. (A1) using data from DSC runs at 80, 100 and 120 °C are displayed in Fig. 12. Before diffusion controlled propagation and decreasing f commence, R_r is proportional to $[R]$:

$$R_r = \frac{1}{1-\alpha}\frac{d\alpha}{dt} = k_p[R] \tag{A1}$$

$d(R_r)/dt$ is proportional to $d[R]/dt$, which is given by Eq. (4). Inspection of Eq. (4) reveals that a decrease in $d(R_r)/dt$ can

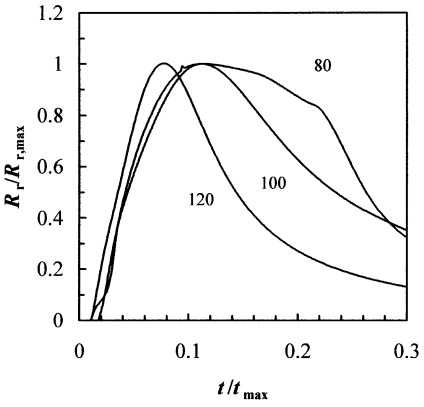

Fig. 12. Normalised reduced reaction rate $R_r/R_{r,max}$ plotted vs. normalised time, t/t_{max} for 80, 100 and 120 °C.

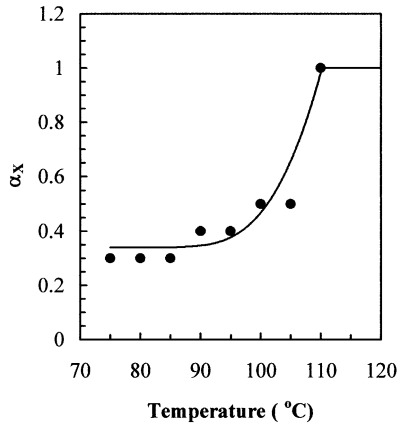

Fig. 14. The parameter α_x of the initiator efficiency model plotted vs. isothermal cure temperature.

be caused by either a decrease in f and/or by a decrease in the initiator concentration. In order to investigate which of these two factors is mainly responsible, simulations were carried out based on Eqs. (3)–(5). It was found that initiator depletion alone is not the cause of the decrease in $d(R_r)/dt$ which can be observed at a fairly low conversion experimentally. The effect is negligible for $t/t_{max} < 0.2$, which is where the decrease in $d(R_r)/dt$ occurs in the experimental data (Fig. 10). The onset of the diffusion-limited effects appears to be independent of temperature in the range investigated. Thus, the average value of α_D ($\alpha_D = 0.016$) was used in the modelling studies. The earlier evidence is not conclusive proof that the decrease in $d(R_r)/dt$ is actually indicative of the onset of decreasing f. If diffusion control of the propagation reaction begins before f starts to decrease, then that could cause a decrease in $d(R_r)/dt$.

It is possible to adjust the expression for f in an empirical manner by selecting values of α_x that gives the most plausible shape for F at each isothermal cure temperature, i.e. F should begin to decrease at α_R (but never increase with increasing conversion). A series of predictions of the way F changes with conversion for different values of α_x at 100 °C are displayed in Fig. 13. Only the conversion-dependences of F matters since its absolute computed value depends on the value given to the parameter k_{p0}, an unknown quantity; the absolute value of f_1 has no effect on the selection of α_x. A polynomial with an imposed minimum of 0.34 and maximum of one was fitted to the data points (Fig. 14).

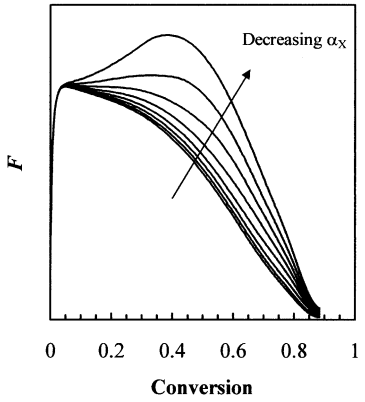

Fig. 13. F calculated from Eqs. (3)–(5) and (19) (with α and $d\alpha/dt$ from DSC data) vs. conversion for $f_1 = 0.6$ and $\alpha_x = 0.3$, 0.4, 0.5, 0.6, 0.7, 0.8, 0.9 and 1 at 100 °C.

References

[1] Malik M, Choudhary V, Varma LK. J Macromol Sci-Rev Macromol Chem Phys 2000;C40:139.
[2] Yang YS, Lee LJ. Polym Process Eng 1987;5:327.
[3] Flory PJ. J Am Chem Soc 1941;63:3083, see also p. 3091, 3096.
[4] Stockmayer WH. J Chem Phys 1944;12:125.
[5] Matsumoto A. Adv Polym Sci 1995;123:41.
[6] Acitelli MA, Prime RB, Sacher E. Polymer 1971;12:335.
[7] Kamal MR, Sourour S. Polym Engng Sci 1973;13:59.
[8] Prime RB. Polym Engng Sci 1973;13:365.
[9] Siegmann A, Narkis M. J Appl Polym Sci 1977;24:2311.
[10] Ryan ME, Dutta A. Polymer 1979;20:203.
[11] Dutta A, Ryan ME. J Appl Polym Sci 1976;24:635.
[12] Han CD, Lem KW. J Appl Polym Sci 1983;28:3155.
[13] Lem KW, Han CD. J Appl Polym Sci 1983;28:3207.
[14] Martin JL, Cadenato A, Salla JM. Thermochim Acta 1997;306:115.
[15] Auad ML, Aranguren MI, Elicabe G, Borrajo J. J Appl Polym Sci 1999;74:1044.
[16] Lin C-M, Weng C-I. Polym Engng Sci 2000;40:290.
[17] Yousefi A, Lafleur PG, Gauvin R. Polym Comp 1997;18:157.
[18] Vilas JL, Laza JM, Garay MT, Rodriguez M, Leon LM. J Appl Polym Sci 2001;79:447.
[19] Stevenson JF. Polym Engng Sci 1986;26:746.
[20] Han CD, Lee D. J Appl Polym Sci 1987;33:2859.
[21] Ng H, Manas-Zloczower I. Polym Engng Sci 1989;29:1097.
[22] Batch GL, Macosko CW. J Appl Polym Sci 1992;44:1711.
[23] Yun Y-M, Lee S-J, Lee K-J, Lee Y-K, Nam J-D. J Polym Sci, Part B Polym Phys 1997;35:2447.
[24] Zetterlund PB, Johnson AF. Thermochim Acta 1996;289:209.
[25] Huang YJ, Lee LJ. AIChE J 1985;31:1585.
[26] Ma SC, Lin HL, Yu TL. Polym J 1993;25:897.
[27] Zetterlund PB. PhD Thesis, University of Leeds, 1997.
[28] Lucas CJ, Borrajo J, Williams RJJ. Polymer 1993;34:3216.
[29] Moze A, Malavasic T, Vizovisek I, Lapanje SD. Angew Makromol Chem 1975;46:89.

[30] Chapra SC, Canale RP. Numerical methods for engineers. 2nd ed. New York: McGraw-Hill Book Company, 1988.
[31] Gill PE, Murray W. Numerical methods for constrained optimisation. London: Academic Press, 1974.
[32] Yang YS, Lee LJ. Polymer 1988;29:1793.
[33] Dell'Erba R, Martuscelli E, Musto P, Ragosta G. Polym Networks Blends 1997;7(1):1.
[34] Tollens FR, Lee LJ. Polymer 1993;34:29.
[35] Yamada B, Westmoreland DG, Kobatake S, Konosu O. Prog Polym Sci 1999;24:565.
[36] Hsu CP, Lee LJ. Polymer 1993;34:4506.
[37] Hill RR, Muzumdar SV, Lee JL. Polym Engng Sci 1995;35:852.
[38] Russell GT, Napper DH, Gilbert RG. Macromolecules 1988;21:2141.
[39] Zetterlund PB, Yamazoe H, Yamada B, Hill DJT, Pomery PJ. Macromolecules 2001;34:7686.
[40] Buback M, Huckestein B, Kuchta F-D, Russell GT, Schmid E. Macromol Chem Phys 1994;195:2117.
[41] Moad G, Rizzardo E, Solomon DH, Johns SR, Willing RI. Makromol Chem Rapid Commun 1984;5:793.
[42] Solomon DH, Moad G. Makromol Chem Macromol Symposia 1987;10/11:109.
[43] Cohen MH, Turnbull D. J Chem Phys 1959;31:1164.
[44] Bueche F. Physical properties of polymers. 1st ed. New York: Wiley, 1962. p. 354.
[45] Simha R, Boyer RF. J Chem Phys 1962;37:1003.
[46] Boyer RF, Simha R. J Polym Sci Polym Lett Ed 1973;11:33.
[47] Hale A, Macosko CW, Bair HE. Macromolecules 1991;24:2610.
[48] Hale A. PhD Thesis, University of Minnesota, 1988.
[49] Ramis X, Salla JM. J Polym Sci, Part B Polym Phys 1997;35:371.
[50] Vilas JL, Laza JM, Garay MT, Rodriguez M, Leon LM. J Polym Sci, Part B Polym Phys 2001;39:146.
[51] Muzumdar SV, Lee LJ. Ann Tech Conf-Soc Plast Engng 1991:737.
[52] Scott EP, Saad Z. Polym Engng Sci 1993;33:1157.
[53] Batch GL, Macosko CW. Society of Plastics Engineers Annual Technical Conference 1987.
[54] Buback M, Kuchta F-D. Macromol Chem Phys 1997;198:1455.
[55] Beuermann S, Buback M. Pulsed laser experiments directed toward the detailed study of free-radical polymerisations. In: Matyjaszewski K, editor. Controlled Radical Polymerisation, ACS Symposium Series 685, 1998 (Chapter 6).
[56] Buback M. Macromol Chem Phys 1990;191:1575.
[57] Buback M, Huckestein B, Russell GT. Macromol Chem Phys 1994;195:539.
[58] Horie K, Mita I, Kambe H. J Polym Sci Part A-1 1970;8:2839.